1

Introduction

1.1 Historical background

The foundations of modern gaseous detectors can be traced back to the works of Ernest Rutherford, 1908 Nobel Laureate in Chemistry. In the course of his studies of the atomic structure, he conceived an instrument capable of detecting individual ionization trails left in a gas by natural radioactivity. Knowledgeable of John Sealy Townsend's studies on collisional charge multiplication in gases at high electric fields, and with the help of Hans Geiger, he built a tool capable of amplifying the weak primary ionization signal. The device consisted of a thin metal wire, the anode, coaxial with a gas-filled cylindrical cathode; on application of a potential difference between the electrodes, electrons released in the gas drift towards the anode, undergo inelastic ionizing collisions in the fast increasing field and multiply in an appropriately named electron–ion avalanche. Restricted to a narrow region around the wire, the multiplication process amplifies the charge released in most of the gas volume and yields a signal proportional to the primary charge, hence its name 'proportional counter' (Rutherford and Geiger, 1908). Large multiplication factors, or gains, could be achieved, permitting the detection of small amounts of primary charge with the rudimentary electrical instrumentation available at the time. Further developments of the device by Geiger and Walther Müller permitted them to reach the ultimate goal of detecting single electrons released in the counter's gas (Geiger and Müller, 1928).

Proportional counters of various sizes and shapes were employed for decades in the detection of ionizing radiation; Geiger–Müller counters are still widely used for radiation monitoring. Arrays of proportional counters have been built to cover larger areas; however, limited in location to their physical size, they could hardly satisfy the tracking requirements of the emerging high-energy particle physics. Already in the 1930s, this goal was mainly achieved using photographic emulsions, capable of recording the trails left by the passage of charged particles.

https://doi.org/10.1017/9781009291200.003 Published online by Cambridge University Press

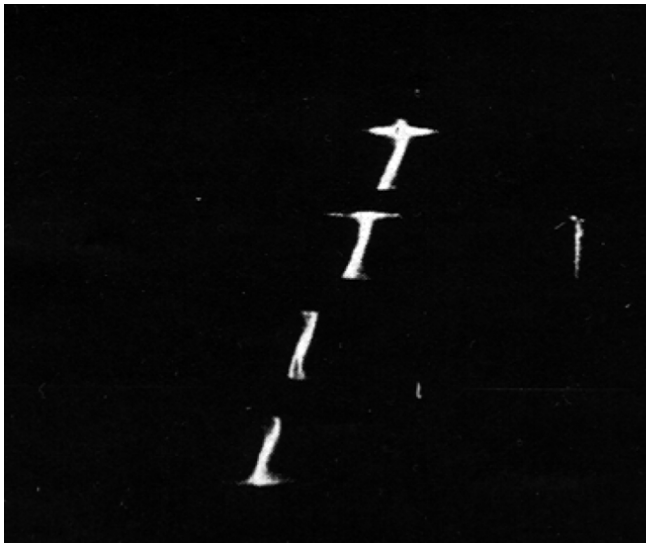

Figure 1.1 A cosmic ray detected in a four-gap spark chamber (Fukui and Miyamoto, 1959). By kind permission of Springer Science+Business Media.

The development of other types of detector having excellent imaging capability, such as the cloud chamber (Charles Thomson Wilson, 1927 Nobel Laureate) and the bubble chamber (Donald Arthur Glaser, 1960 Nobel Laureate), relegated the use of emulsions to specialized nuclear physics investigations. Bubble chambers, at the same time target and detector and providing accurate three-dimensional optical images of complex events, were successfully used for decades in particle physics and still powerful tools of investigation in the 1960s. However, these devices have a major drawback: they are made sensitive under the action of an external mechanical control only during a selected time interval, uncorrelated to the physical events under study. Well adapted to the analysis of frequent processes, they are less suited for the study of rare events.

A new type of gas counter that could be made sensitive in coincidence with selected events, the triggered spark chamber, was developed in the late fifties (Fukui and Miyamoto, 1959). On application, shortly after the passage of a charged particle, of a high voltage pulse across a thin gas layer between two electrodes, a detectable spark would grow along the ionization trails left in the gas. A system of external coarse devices, as a set of scintillation counters, provides a signal to trigger the chambers in coincidence with specific geometrical or energy loss requirements; the concept of selective event trigger was born.

Figure 1.1, from the reference above, is one of the first pictures of a cosmic ray track detected with a four-gap spark chamber. Stacks of thin-gap spark chambers could thus provide a sampled image of tracks crossing the detector within a short

https://doi.org/10.1017/9781009291200.003 Published online by Cambridge University Press

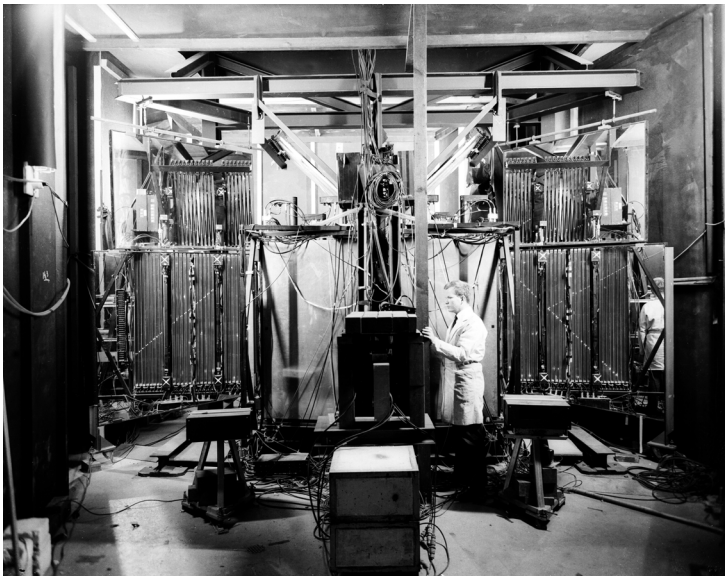

Figure 1.2 PS11, an optical spark chamber experiment at CERN's Proton Synchrotron, with accidental cosmic rays tracks. Picture CERN (1967).

time window, and were extensively used in particle physics experiments, cosmic ray studies and other applications. Recording of the events was done by photography or, in the later times, electronic video digitization. Figure 1.2 is an example of an experimental setup with several optical spark chamber stacks surrounding a target, operating in the 1960s at CERN.

Limited originally by the slow picture recording process, spark chambers evolved into faster electronic devices thanks to the development of methods capable of detecting the current pulse produced by a spark on electrodes made with thin wires. The most successful employed small ferrite core beads, used at the time in computer memories, interlaced with the wires and read out with a sequence of electrical pulses (Krienen, 1962). Simple to implement, the magnetostrictive readout method, introduced in the early sixties, relied on the detection of the sonic waves induced by a discharge on an external wire transducer, perpendicular to the wire electrodes; coordinates were then deduced from the time lapse between the spark and the detection of the sound pulse at the two ends of the pickup wire (Perez-Mendez and Pfab, 1965). Other methods included capacitive charge storage and direct detection of the spark sound with microphones located in strategic positions; for a review see for example Charpak (1970).

In thin-gap chambers, the applied high voltage pulse causes a discharge propagating from anode to cathode. Further developments of the technology led to the introduction of a more powerful family of devices, named streamer chambers: these

https://doi.org/10.1017/9781009291200.003 Published online by Cambridge University Press

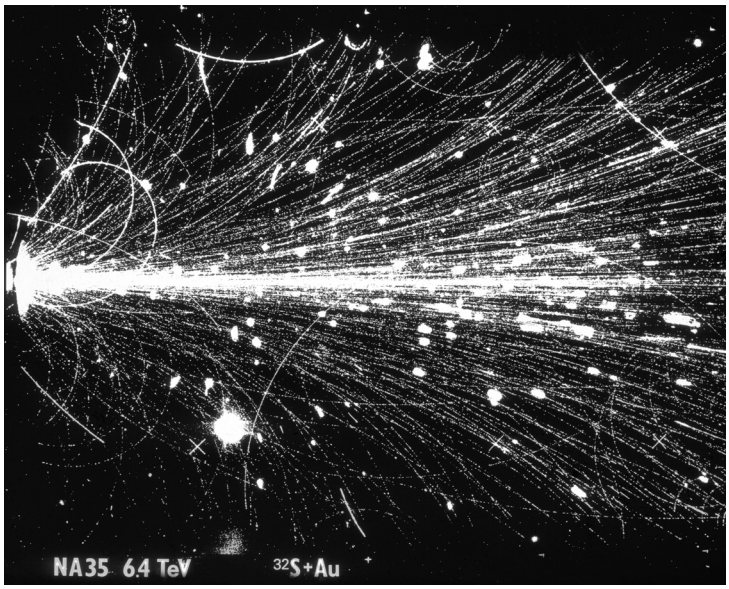

Figure 1.3 Heavy ion collision recorded with CERN's NA35 streamer chamber. Picture CERN (1991).

are large volume detectors in which a very narrow and high voltage pulse induces the formation of short local discharges following the ionized trails in the gas. While having rate capability limited to a few hertz, needed to generate nanosecond-long, hundreds of kV/m voltage pulses, the streamer chambers had an impressive multi-track imaging capability, as shown by the example of Figure 1.3, recorded with the NA35 streamer chamber at CERN on a relativistic heavy ion collision (Brinkmann *et al.*, 1995). In many ways, later developments with gaseous detectors, the main subject of this book, have been inspired by the challenge to achieve similar image qualities with faster, fully electronic devices. For a review of streamer chambers development and performances see Rohrbach (1988).

1.2 Gaseous detectors: a personal recollection

In the late 1960s, as a post-doc at the University of Trieste (Italy), I contributed to the realization of a detector system using wire spark chambers with magnetostrictive readout, used in an experiment at CERN. While a technical staff was in charge of the chamber's construction, the delicate but tedious work of winding the miniature coils used to detect the sonic pulse on the acoustic sensing wire was a task for the young students. The results of the test beam measurements of efficiency and position accuracy with a set of detectors are described in my first

https://doi.org/10.1017/9781009291200.003 Published online by Cambridge University Press

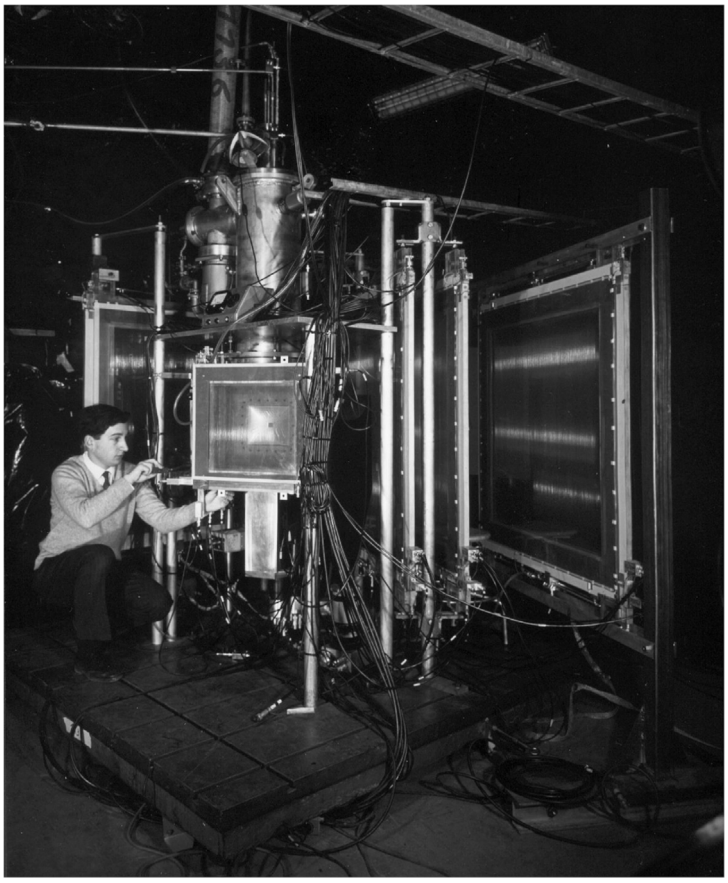

Figure 1.4 The author with the CERN–Trieste magnetostrictive spark chambers setup. Picture CERN (1967).

publication (Bradamante and Sauli, 1967); I can be seen in in Figure 1.4 working on the experimental setup, a fixed target experiment to study proton–proton and proton–deuteron interactions at (for that time) high energies.

Albeit selective and faster in response than previous generations of detectors, spark chambers are limited in operating rate to a few tens of hertz, due to the time needed to clear the excited and ionized species from the region of a spark before the application of another pulse, in order to prevent re-firing.

In the late 1960s, the need for large area and faster electronic detectors acquired paramount importance, motivated by the challenging requirements of the increasingly high-energy particle physics. The multi-wire proportional chamber (MWPC), invented in 1967 by CERN's Georges Charpak, revolutionized the field of position-sensitive detectors (Charpak *et al.*, 1968). In Figure 1.5 Charpak's technician, Roger Bouclier, stands next to the first MWPC, with 24 anode wires

https://doi.org/10.1017/9781009291200.003 Published online by Cambridge University Press

Figure 1.5 Roger Bouclier with the first multi-wire proportional chamber. Picture CERN (1968).

and 10×10 cm^2 active area.[1] For his invention, and the contribution of the new family of detectors to fundamental research, Charpak received the 1992 Nobel Prize for Physics.

The outstanding innovative performances of the new device were soon recognized, despite the challenge posed at the time by the need of using individual recording electronic channels on many wires a few mm apart: nanosecond time resolution, sub-mm position accuracy, continuous sensitivity and high rate capability. The new detector technology, swiftly adopted by several experiments, gave Charpak resources and support to continue and expand the research activity on gaseous detectors. I joined Charpak's group in 1969, contributing for many years to the development and applications of innovative gaseous detectors; after Georges' retirement in 1989, I took the leadership of the group then named Gas Detectors Development (GDD) until my own retirement in 2006. During all those years, the continuing challenge posed by the increasing requirements of particle

[1] There is no known picture of Charpak himself with the early MWPCs; Figure 1.8, taken several years later, is sometimes quoted to be one.

https://doi.org/10.1017/9781009291200.003 Published online by Cambridge University Press

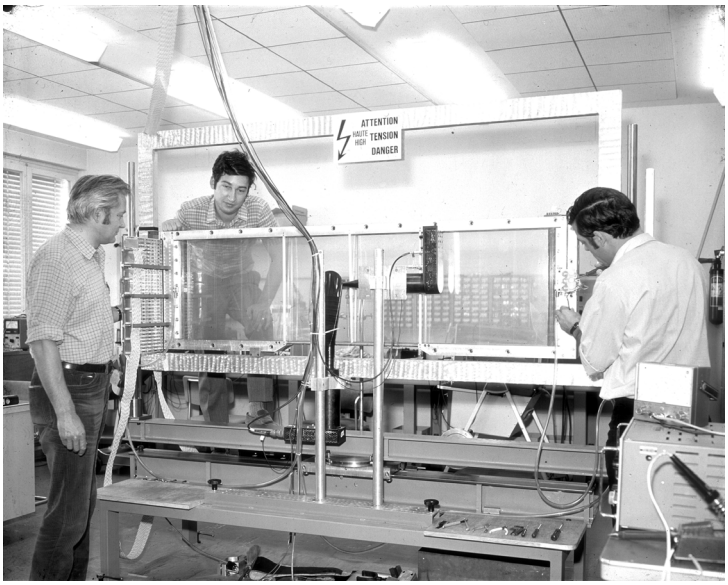

Figure 1.6 A large MWPC prototype, with (left to right) Georges Charpak, Fabio Sauli and Jean-Claude Santiard. Picture CERN (1970).

physics experimentation motivated the search for faster and more performing devices that exploit the properties of charge transport and multiplication in gases.

The original MWPC could attain avalanche gains around 10^5; detection of the signal released by fast particles (a few tens of electron–ion pairs) required the use of low noise amplifiers, which was possible but rather demanding for the electronics of the time. A major discovery by Charpak's group, and possibly a reason for the fast spread of the technology, was a gas mixture in which saturated gains above 10^7 could be reached, providing pulses of amplitude independent of the primary ionization release, thus leading to simpler requirements for the readout electronics. Quite appropriately, this mixture (argon-isobutane with a trace of freon) was named 'magic gas' (Bouclier *et al.*, 1970).

The first MWPC was only 10 cm on the side; soon, a large effort was put into developing the technology for manufacturing larger detectors. However, unexpected problems of electrostatic instability, discussed in Section 8.4, resulted in a dramatic failure of the early prototypes; the problem was solved with the introduction of internal insulating supports or spacers. Figure 1.6 shows one of the first large size working devices, about one and a half metres on the side, built by the group in 1970 (Charpak *et al.*, 1971).

Suitable for fixed target experiments, the heavily framed construction of the chamber seen in the picture was not optimal for use within a magnet, due to the unfavourable ratio of active to total area; a lighter design of the detector, which

https://doi.org/10.1017/9781009291200.003 Published online by Cambridge University Press

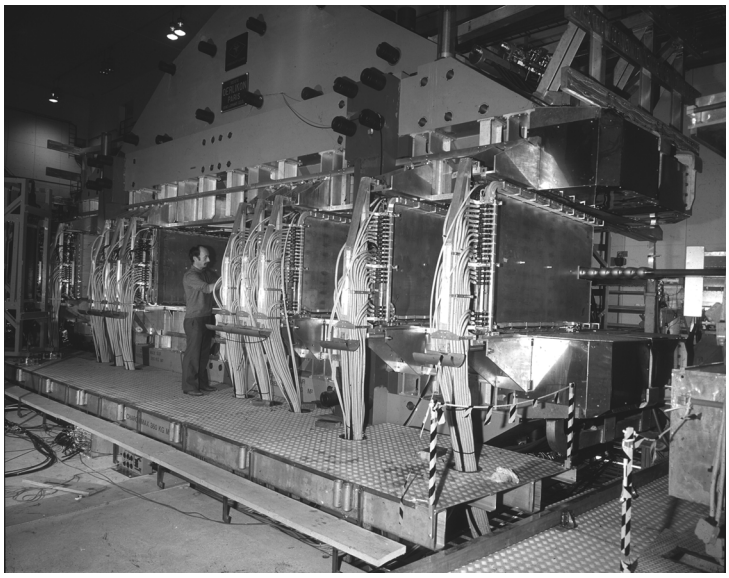

Figure 1.7 The 40 MWPC array of the Split Field Magnet Detector spectrometer. Picture CERN (1973).

made use of self-supporting, light honeycomb panels holding the wires, was developed by the group to equip the multi-particle spectrometer of the Split Field Magnet experiment at CERN's proton–proton storage rings (Figure 1.7) (Bouclier *et al.*, 1974). Deploying 40 large MWPC modules, the instrument featured data taking rates of several kHz, a performance unthinkable when using older tracking devices, and operated for many years for systematic measurements of particle yields in proton–proton collisions. One of the searches, the quest for free quarks, yielded no results for fundamental reasons that become clear only later; however, it motivated one of my early works to estimate the detection efficiency of MWPC on charge 1/3 particles (Breidenbach *et al.*, 1973).

In the initial conception of the MWPC, space accuracy was determined by wire spacing, a few mm at best. As anticipated in seminal work by Charpak and collaborators, sub-mm position accuracies could be achieved by exploiting the time lag, or drift time, of the detected charge in respect to an external trigger (Charpak *et al.*, 1970). Developed in the early seventies, and using several centimetres wire spacing, drift chambers provided position accuracies between 300 and 400 μm, while substantially reducing the number of electronics channels (Walenta, 1973). A thorough optimization of the electric field structure and detailed studies on the electrons' drift properties permitted them to reach position accuracies around 50 μm for fast particles perpendicular to the detector (Charpak *et al.*, 1973). Figure 1.8 shows Charpak with an early prototype of the High

https://doi.org/10.1017/9781009291200.003 Published online by Cambridge University Press

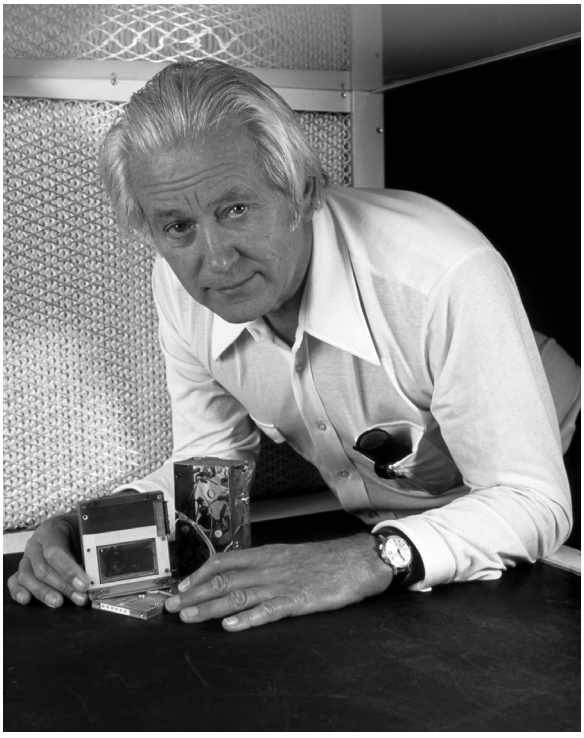

Figure 1.8 Georges Charpak with the first prototype of the high accuracy drift chamber. By permission of SPL Science Photo Library (1982).

Accuracy Drift Chamber, a single cell 50 mm wide; curiously, in the absence of a picture of the inventor with the first MWPC, this picture is sometimes referred to as such. In Figure 1.9, Guy Schultz and Amos Breskin, former members of the group, are seen inserting a set of medium-size high accuracy drift chamber prototypes in a magnet for systematic measurements of performances in magnetic fields. As will be discussed in more detail in Chapter 9, each chamber provided two perpendicular coordinates, resolving the right–left ambiguity, intrinsic in a time measurement, thanks to the use of anode wire doublets mounted at a close distance.

The temperature dependence of the drift properties, crucial for a stable long-term use of the devices, was studied thoroughly with dedicated detectors, and led to the choice of operating gases having a saturated drift velocity, with minimal variation with temperature (see Section 4.7). Requiring the heating of the detectors while operating, these studies resulted often in spectacular failures due to the appearance of heavy discharges in flammable gas mixtures (Figure 1.10).[2]

[2] This event is colloquially named 'Breskin's thermodynamics experiment' from the name of the team member in charge of the measurement.

https://doi.org/10.1017/9781009291200.003 Published online by Cambridge University Press

Figure 1.9 Guy Schultz (left) and Amos Breskin (right) inserting a set of high accuracy drift chambers in a magnet. Picture CERN (1972).

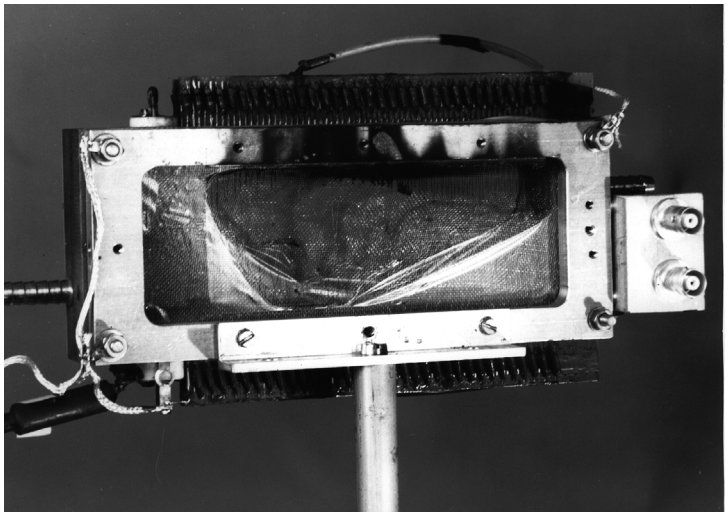

Figure 1.10 Burned-out drift chamber, the end of a temperature dependence study. Picture by the author at CERN (1972).

https://doi.org/10.1017/9781009291200.003 Published online by Cambridge University Press

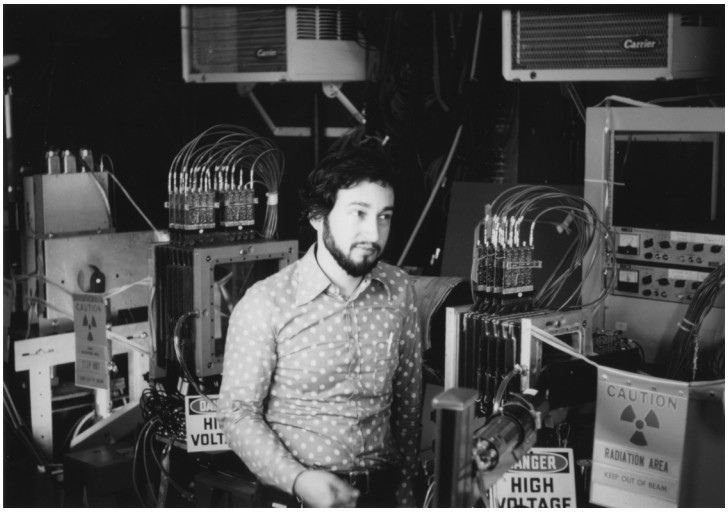

Figure 1.11 The JINR high-accuracy drift chamber setup at Fermilab. Picture by the author (Sauli, 1977).

The unique position accuracy properties of the detectors were soon exploited in experiments. I participated in the initial study of the kaon form factor in a K-e scattering experiment at Fermi National Laboratory in Batavia by a group of the Joint Institute of Nuclear Research (JINR Dubna) led by Edick Tsyganov (Filatova *et al.*, 1977); in Figure 1.11 I pose with the two drift chamber telescopes of the experiment installed in a beam line at Fermilab.

Another experiment exploiting the excellent space localization properties of our drift chambers was the study of channelling effects of fast charged particles in crystals, set up at CERN by a group from Aarhus University (Denmark). Figure 1.12 is a stereogram of the distribution of incidence angle of 1.35 GeV π^+ on a germanium crystal, selected for releasing less than average energy in the crystal, clearly showing an increase of the yield along the crystal axis and planes (Esbensen *et al.*, 1977). The study of channelling properties in crystals continued for many years, eventually focussing on the possibility of deflecting high-energy particle beams using bent crystals (Tsyganov, 1976) and is a subject of continuing investigation, see for example Chesnokov *et al.* (2013) and references therein.

In the mid-1970s we used a set of high-accuracy drift chambers to investigate the prospects of exploiting the reconstruction of the vertex of interaction of high energy protons within a target, thus obtaining a three-dimensional density map, with the so-called nuclear scattering radiography method (NSR)[3] (Saudinos *et al.*, 1975).

[3] Given its full 3-D imaging capability, the method would be more appropriately named nuclear scattering tomography.

https://doi.org/10.1017/9781009291200.003 Published online by Cambridge University Press

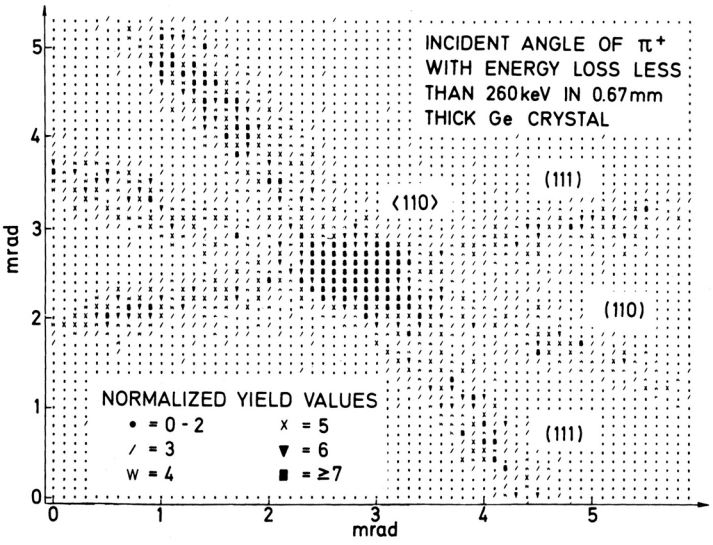

Figure 1.12 Angular distribution of 1.35 GeV pions releasing less than the average energy loss in a germanium crystal (Esbensen *et al.*, 1977). By kind permission of Elsevier.

The measurements demonstrated the feasibility of a diagnostic tool that provided good image quality at low patient irradiation doses compared to X-ray tomography; tagging of the proton–proton elastic scattering component, with a simple angular correlation cut, permitted the identification of the hydrogen content in the body (see Figure 1.13).

Requiring the use of ~GeV proton beams, available in only a few high energy physics research centres, the NSR method remained for many years a curiosity. It has, however, been reconsidered as a tool for quality assurance at the upcoming oncological hadrontherapy centres, exploiting the high energy proton and ion beams used for deep neoplasm treatment (see the end of this section).

Concurrently with the development of high-accuracy drift chambers, a detailed study of the processes of signal induction on electrodes led to the introduction of a method of localization based on the recording of the signals induced by the avalanches on cathodes (Charpak and Sauli, 1974). Unlike drift chambers, which require an external time reference to perform localization, cathode-readout MWPC can be self-triggered by the anodic signal, thus making the device suitable for detection and localization of short-range and neutral radiation. An example of application for radio-chromatography, the two-dimensional activity distribution in a sliced tritium-labelled rat brain is shown in Figure 1.14 (Dominik *et al.*, 1989).

https://doi.org/10.1017/9781009291200.003 Published online by Cambridge University Press

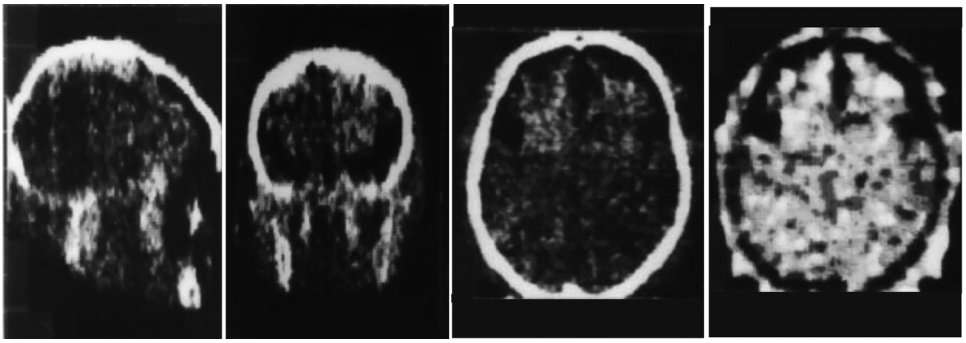

Figure 1.13 Nuclear scattering radiography: 3-D reconstruction of the density distribution on slices through a human head. The rightmost image corresponds to selected p-p elastic scatter events (Duchazeaubeneix *et al.*, 1980). By kind permission of Wolters Kluwer Health.

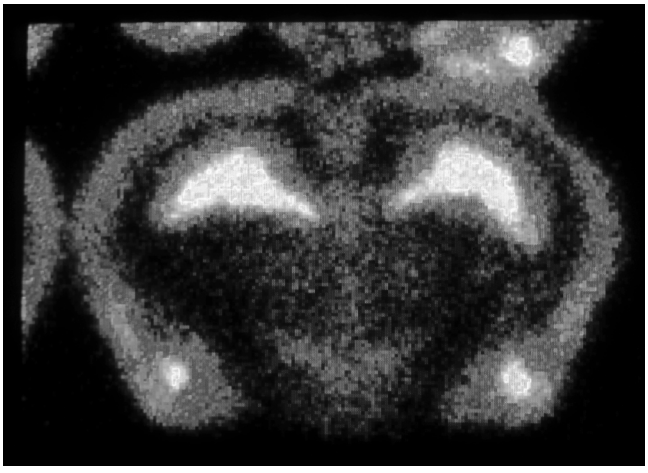

Figure 1.14 Radio-chromatography of a tritiated slice of a rat's brain (Dominik *et al.*, 1989). By kind permission of Elsevier.

Many variants of the two-dimensional MWPC have been developed for the needs of particle physics experimentation, and will be described in the next chapters, the most powerful being perhaps the time projection chamber developed by David Nygren and collaborators in the late 1970s (Nygren and Marx, 1978); for a review see for example Sauli (1992).

Introduced by Thomas Ypsilantis and Jacques Séguinot in the late 1970s (Seguinot and Ypsilantis, 1977), the Cherenkov ring imaging (RICH) technique is a particle identification method based on the detection and localization of UV photons emitted in a radiator by the Cherenkov effect with a gaseous counter.

https://doi.org/10.1017/9781009291200.003 Published online by Cambridge University Press

Figure 1.15 Philippe Mangeot and Anna Peisert with one of the photon detectors of the E605 RICH at Fermilab. Picture by the author (1980).

Using a photosensitive gas filling, these detectors are prone to suffer from photon-induced feedback problems when operated at the high gains needed for detection of single photoelectrons, due to the copious emission of photons by the avalanches. Developed in 1978 by Charpak and myself, the multi-step avalanche chamber (MSC) solved the problem (Charpak and Sauli, 1978). The MSC combines in the same device a region of high field between two semi-transparent meshes, and a standard MWPC, separated by a low-field gap. A fraction of the electrons created in the first multiplier transfers to the second and multiplies again, permitting the desired high gain; with a proper choice of the photosensitive gas concentration, photons emitted by the avalanches in the MWPC are absorbed before reaching the first amplifier and do not induce the formation of secondary avalanches (Charpak *et al.*, 1979a).

Built by a CERN–CEN–Saclay collaboration, two UV-photon sensitive MSCs mounted on a helium-filled radiator operated for several years as the Cherenkov ring imaging particle identifier of the experiment E605 at Fermilab (Adams *et al.*, 1983); with a 3-D projective readout (the anodes and two sets of angled cathode wires), the detector achieved ambiguity-free localization of multiple photoelectrons in a ring pattern. The picture in Figure 1.15 shows two members of the group next to one of the UV-photons sensitive chambers; performances of the detectors are discussed in Section 14.3.

The first generation of RICH detectors used vapours of triethyl amine (TEA) added to the gas mixture as photosensitive agent; due to its ionization threshold in

https://doi.org/10.1017/9781009291200.003 Published online by Cambridge University Press

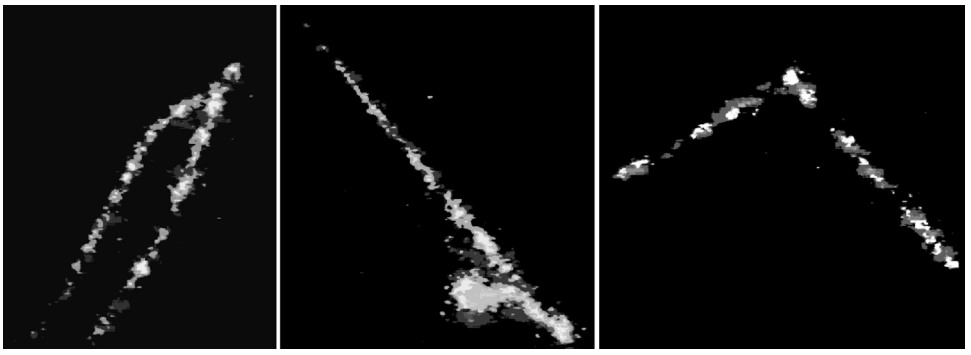

Figure 1.16 Cosmic rays recorded with the optical imaging chamber (Charpak *et al.*, 1987). By kind permission of Elsevier.

the far UV (7.5 eV), TEA requires the use of expensive fluoride windows to separate detector and radiator. A substantial improvement in the technology was made possible when David Anderson, who joined our CERN group in 1983, brought in samples of TMAE, a product with the amazingly low ionization threshold in the vapour phase of 5.4 eV; this permitted the use of quartz windows, and led to the construction of large acceptance RICH particle identifiers at CERN and elsewhere (see Section 14.4).

The research on low photo-ionization threshold vapours had an interesting spin-off: it was found that these compounds also act as efficient internal wavelength shifters, copiously emitting photons at wavelengths near to or in the visible range, easy to detect and image with optical means (see Section 15.1). In the imaging chambers, the ionized trails drift to an end-cap multiplier in conditions optimized to obtain a large scintillation yield; a solid-state camera records the projected images through the detector window (Charpak *et al.*, 1987). The detectors are continuously active, limited in rate capability only by the image acquisition hardware. Examples of cosmic ray activity recorded with an optical imaging chamber are shown in Figure 1.16. A chamber producing images visible to the naked eye, colloquially named 'Charpaktron', operated for some time in CERN's permanent exhibition Microcosm.[4]

Other applications of the optical imaging chambers include autoradiography of radioactive compounds (Dominik *et al.*, 1989) and detection of low-energy nuclear decays (Miernik *et al.*, 2007). As demonstrated in the last reference, the scintillation intensity is proportional to the ionization density, and the detector can be used for quantitative measurements of the energy loss as well as the interaction topology.

[4] Requiring several minutes of adaptation in the dark, the device was not a top hit with visitors, and was eventually discontinued.

https://doi.org/10.1017/9781009291200.003 Published online by Cambridge University Press

Mass-produced in a variety of sizes and shapes, and integral components in many experimental setups, MWPCs have, however, some limitations intrinsic in their conception. The delicate stringing and the fragility of the thin anode wires affect the reliability; the production of various kinds of deposits on the electrodes in the charge multiplication processes results in a long-term deterioration of the detectors. More fundamentally, while localization accuracies of 50–100 μm can be achieved with a measurement of the drift time or of the cathode induced charge profiles, this goes at the expense of the multi-track resolution, which is around 10 mm at best. The rate capability of MWPCs is also limited to a few kHz/mm^2 by the build-up of a positive ion space charge, dynamically modifying the electric fields.

In 1988 at the Institute Laue-Langevin (ILL) in Grenoble, Anton Oed developed a new detector concept named micro-strip gas counter (MSGC), which promised to improve both the multi-track resolution and the rate capability by at least one order of magnitude (Oed, 1988). The MSGC structure consists of thin parallel metallic strips engraved on a glass substrate and alternately connected as anodes and cathodes. Strip widths are typically of 10 and 50 μm for anodes and cathodes respectively, at 100 μm distance; a drift electrode provides gas tightness and completes the detector. Thanks to the narrow pitch of the strips and to the fast collection of the majority of the positive ions by the closer cathode strips, the MSGC can operate efficiently at radiation fluxes above one MHz/mm^2, with localization accuracies and multi-track resolutions for fast particles around 50 μm and 500 μm, respectively (see Section 13.1).

The exceptional performances of the new device attracted considerable interest; I acted as spokesperson of the CERN-based international collaboration RD-28, approved in 1992 and aiming at the development of the MSGC technology.[5] Figure 1.17 shows one of the MSGC detectors, fully equipped with readout electronics, part of a setup built by the GDD group under my leadership, and used for systematic performance studies in high intensity beams (Barr *et al.*, 1998).

However, experience has shown that the detectors were rather fragile; because of the high electric field strength on the strips' edges, the avalanche charge occasionally grows large enough to exceed the so-called Raether limit and induce discharges (see Section 8.8). As an example, Figure 1.18 is a close view of a fresh, slightly pitted and seriously damaged MSGC plate after use. Despite a large effort dedicated to finding ways to improve the long-term reliability, with only few exceptions MSGC-based detectors were eventually discontinued for most applications.

[5] The research effort continued from 2008 to include other types of high-resolution detector, generically named micro-pattern gas detectors (MPGD) under the label RD-51.

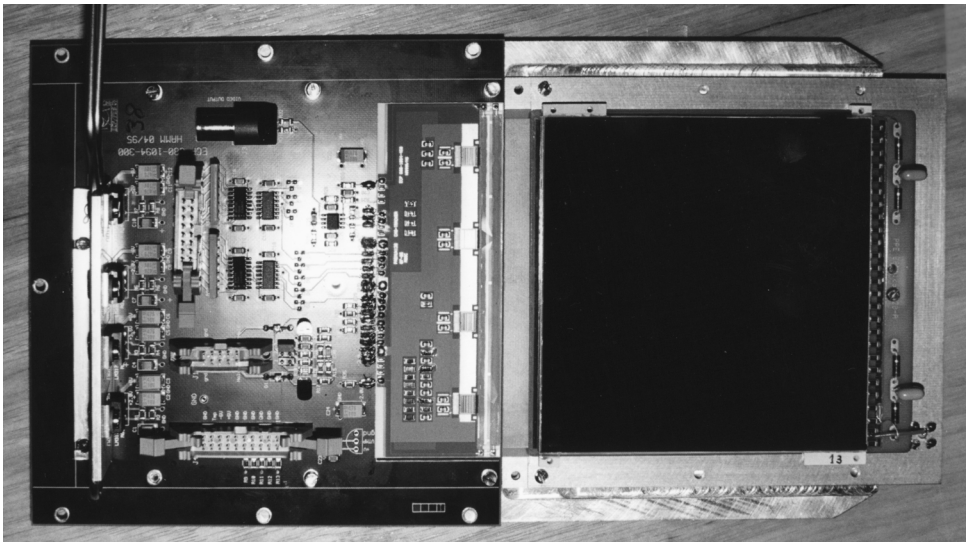

Figure 1.17 A 10×10 cm^2 MSGC detector fully equipped with readout electronics (Barr *et al.*, 1998). By kind permission of Elsevier.

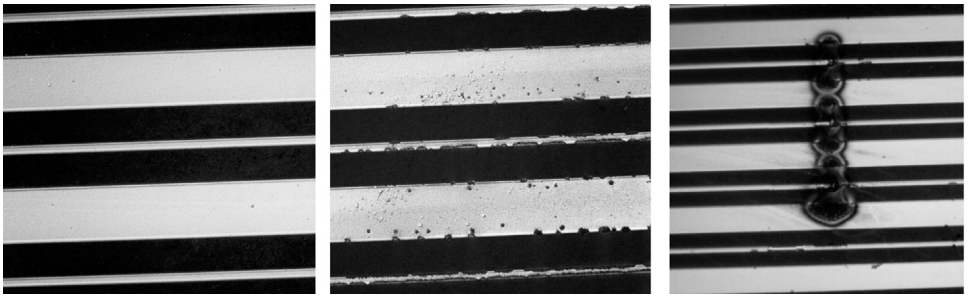

Figure 1.18 Close views of a MSGC plate before use, pitted by a moderate amount of micro-discharges and after a full discharge. Pictures by the author (Sauli, 1998).

The problems encountered with the microstrip detectors encouraged disappointed developers to seek for alternative devices. In 1997 I introduced a new concept, the gas electron multiplier (GEM) (Sauli, 1997), a development pursued by several groups and successfully used in many experiments (see Section 13.4). A GEM electrode is a polymer foil, copper-clad on both sides and with a high density of through-holes, typically 100 per square mm (Figure 1.19). On application of a high voltage gradient between the two sides, and in an appropriate gas environment, electrons released by ionization on one side of the electrode drift into the holes and multiply; most electrons in the avalanche exit the holes and transfer to a second element, another GEM foil or a printed circuit electrode with a pattern

https://doi.org/10.1017/9781009291200.003 Published online by Cambridge University Press

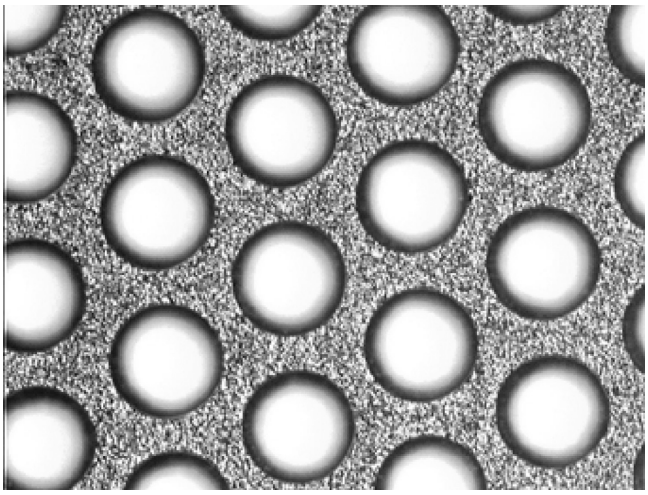

Figure 1.19 Close view of a GEM electrode; typical diameter and distance of the holes are 70 and 140 μm, respectively. Picture by the author (Sauli, 1997).

of strips or pads for charge collection and position readout. Not fortuitously, the structure bears a resemblance to the multi-step chamber described before, albeit at a miniaturized scale.

Offering performances comparable to those of the MSGC, the new device has distinctive advantages: a sturdy construction with a separation of the multiplication and signal pickup electrodes, thus minimizing the likelihood of damage due to discharges; the possibility of cascading several electrodes, in the so-called multi-GEM chamber, permits one to reach very high overall gains and a strong reduction of the positive ions backflow, a paramount feature in GEM-based time projection chambers (see Section 13.5). The readout electrode itself can be patterned at will, a common choice being two sets of perpendicular strips, typically at a few hundred microns pitch, to perform bi-dimensional localization of tracks (Bressan *et al.* (1999c)). An overall signal can be detected on the lower electrode of the last GEM in a cascade, thus providing an energy trigger for selection and recording of neutral radiation.

Manufactured originally with standard printed circuit tools, the early GEM foils had a surface of only a few cm^2; the technology has evolved both at CERN and in industry to satisfy the increasing demand for larger surfaces, reaching at the time of writing almost a square metre.[6] In Figure 1.20 I hold a 30×30 cm^2 GEM foil, one of a large production for the forward tracker of the COMPASS spectrometer at CERN that includes more than 20 medium-size triple-GEM

[6] The surface treatment group, led by Rui de Oliveira, has developed the technology used for the manufacturing of large size GEM electrodes at CERN.

https://doi.org/10.1017/9781009291200.003 Published online by Cambridge University Press

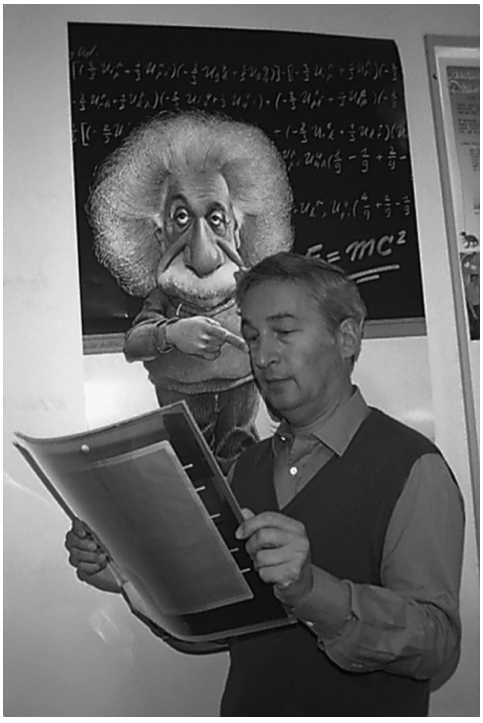

Figure 1.20 The author with a large GEM foil used for the COMPASS tracker. Picture CERN (2001).

detectors (Altunbas *et al.*, 2002). Commissioned in 2002, the tracker was still in operation in 2012.

Owing to their reliability, fast response and high-accuracy localization properties, GEM-based detectors find numerous applications in particle physics, medical diagnostics, astrophysics and other fields (see Section 13.7).

Figure 1.21 is an example of X-ray absorption radiography of a small mammal recorded with a GEM detector (Bachmann *et al.*, 2001).

In an ideal continuance of the nuclear scattering radiography method, I contributed to the development of diagnostics instrumentation aimed at improving the quality assurance in hadrontherapy, the deep tumour treatment with high-energy ion beams. The proton range radiography (PRR) system relies on the measurement of the direction and residual range of particles at energies above full absorption in the patient, and provides a map of the integrated density in the body; in an alternative named interaction vertex imaging (IVI), the same instrument is placed at angles with the beam, and permits one to reconstruct the density of the interaction vertices. Both instruments use medium-size GEM detectors for the measurement of the beam or scattered particles direction (Amaldi *et al.*, 2011; Bucciantonio *et al.*, 2013).

https://doi.org/10.1017/9781009291200.003 Published online by Cambridge University Press

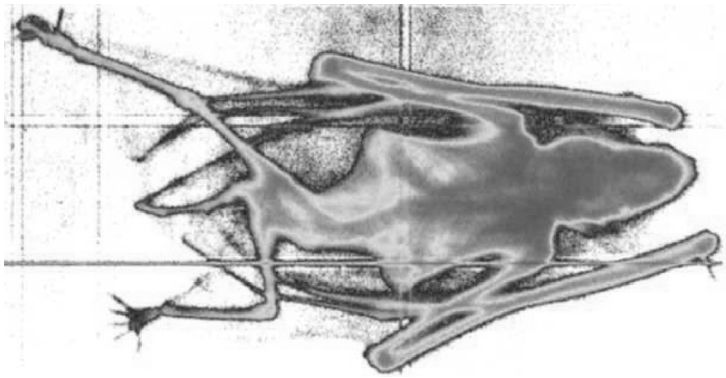

Figure 1.21 Soft X-ray radiography of a bat (image size 70×30 mm^2) recorded with a two-dimensional GEM chamber (Bachmann *et al.*, 2001). By kind permission of Elsevier.

1.3 Basic processes in gaseous counters

The physical processes governing the operation of gaseous counters are discussed extensively in the following chapters. As an introductory help to the novice reader, a short summary of the major events leading to the detection of ionizing radiation is presented here.

The process begins with the release in the gas of one or more ion–electron pairs, in a number and with a distribution that depend on the nature and energy of the radiation; the minimum energy loss required is of course the ionization potential of the concerned atom or molecule. Occasionally, the energy of the primary electrons is sufficient to further ionize the gas molecules, in a cascade of secondary interactions that stops when all the available energy loss is dissipated and the various yields reach thermal equilibrium. For charged particles, the distinction between primary and total ionization is paramount for understanding the detectors' performance. Table 1.1 provides typical values of the number of primary and total ion pairs produced in argon gas at normal conditions by various types of radiation. Needless to say, the larger the release, the more undemanding the requirements on the detector recording electronics; for example, α particles can easily be detected with ionization chambers having no gas gain.

Once released in the gas, electrons and ions may neutralize by mutual recombination or by collisions with the walls; subjected to an external electric field, they separate and migrate towards the electrodes of the counter. The field strength needed for separation depends on the primary ionization density and on the gas, but is typically of a few tens of V/cm in argon at NTP.

When separated, electrons and ions diffuse thermally in the gas volume, bouncing around as an effect of collisions with the molecules, with a global slow motion

Table 1.1 *Examples of ionization yields in argon at NTP of various kinds of radiation.*

Particle	Primary	Total
UV photon	1	1
1 keV X-ray	1	50
100 keV electron	1000 ip/cm	3000 ip/cm
1 GeV proton (minimum ionizing)	25 ip/cm	100 ip/cm
5 MeV α particle	$\sim 10^4$	$\sim 3 \times 10^4$

Table 1.2 *Drift velocity w^+ (w^-) and transverse diffusion σ^+ (σ^-) of ions (electrons), for 1 cm drift in several gases (at NTP) and field values.*

Gas	Field (V cm^{-1})	w^+ (cm ms^{-1})	σ^+ (mm) (1 cm)	w^- (cm μs^{-1})	σ^- (mm) (1 cm)
Argon	100	1.7	0.22	0.24	2.8
	1000	17	0.07	0.45	0.58
CH_4	100	2.2	0.22	1.73	0.29
	1000	22	0.07	10.56	0.24
CO_2	100	1.1	0.22	0.08	0.22
	1000	11	0.07	0.73	0.08

in the direction of the field, named drift velocity. Due to their mass difference, the velocity for ions and electrons at a given field strength differs by several orders of magnitude; moreover, for electrons it strongly depends from the gas and field, as shown by the examples in Table 1.2.

The drift velocity of ions increases almost linearly with the field, up to very high values. On the contrary, for electrons, which can acquire energy from the external field between collisions, the dependence is more complex, often reaching a maximum at fields of a few hundred V/cm, and then saturating or decreasing, depending on the gas mixture. The diffusion has also a strong dependence on the field and gas; some values are given in the table, for 1 cm of drift.

By increasing the field strength, electrons acquire enough energy to induce inelastic processes in their collisions with the gas molecules; in argon at NTP the threshold for the appearance of ionizing collisions is around 10 kV/cm. As a result, new electron–ion pairs are formed, and the charge multiplication process continues in avalanche, with the fast electrons on the front and a tail of slower ions. The resulting voltage–current dependence has a characteristic exponential shape, as shown by the example in Figure 1.22 (Sharma and Sauli, 1992).

https://doi.org/10.1017/9781009291200.003 Published online by Cambridge University Press

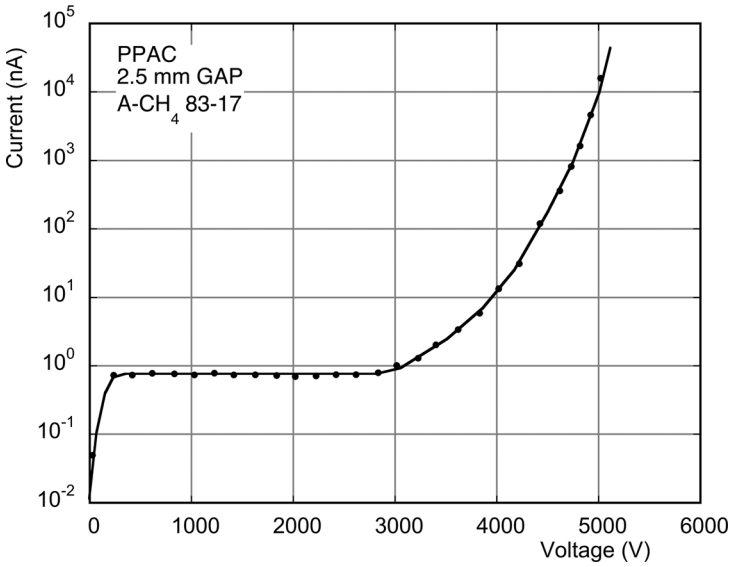

Figure 1.22 Characteristic voltage–current dependence measured in a gaseous counter. The gain, or multiplication factor, of the device is defined as the ratio of the current at a given voltage to the constant value before multiplication (Sharma and Sauli, 1992). By kind permission of Elsevier.

Within a few ns from the start of the multiplication process, all electrons in the avalanche have reached the anode; their collection contributes to the formation of the detected signal. The time taken by ions to reach the cathode, where they are neutralized, is tens to hundreds of μs, depending on the detector geometry and field strength. In their motion, particularly during the initial fast drift in the high field close to the anodes, ions induce charge signals in all electrodes; the (negative) charge induced by ions on the anode constitutes in fact the largest fraction of the detected signal.

Many other processes contribute to the response of a gas counter. In the presence of electro-negative pollutants, the most common being oxygen and water, electrons can be lost by capture. As the attachment cross sections depend on the electron energy, the capture probability is field-dependent; common practice shows that for efficient electron collection, fields above a few hundred V/cm may be needed.

In competition with the charge-amplifying ionizing collisions, atomic and molecular excitation can result in the emission of photons that can generate secondary electrons in the gas or at the electrodes, spreading the original avalanche. At very high gains, these processes can lead to the transition from the avalanche to a streamer, and in extreme cases induce a discharge. All these processes are discussed in detail in the next chapters.

1.4 Outline of the book

The technology of gaseous detectors has been in continuing and fast evolution, mostly thanks to the increasingly demanding requirements of particle physics experimentation. The phenomena describing the release, collection and multiplication of charges, basic in the operation of counters, have been studied extensively in the field referred to as gaseous electronics, and are discussed in numerous textbooks; the information on the newly developed devices is instead scattered in a large number of topical articles and conference proceedings. This book has been conceived as guidance to the field of gaseous radiation detectors, providing the essential data bibliography on their development and applications.

The first chapters describe the major phenomena providing detectable signals in gaseous counters, starting with the processes of energy loss for charged particles and for neutral radiation. The fate of the charges released in the gas is discussed then at increasing values of electric field, from the simple transport to the onset of inelastic collisions and charge multiplication. On each subject, simple approximate calculations based on classic theory are presented whenever possible, and the reader is referred to the more sophisticated and powerful computer programs developed to describe the various processes.

The following chapters then describe the evolution of detectors, from the simple parallel plate and single-wire counters to the more elaborated multi-wire and drift chambers and their siblings. The technologies aimed at realizing coarse very large area detectors and, conversely, smaller but very performing detectors are discussed in detail in the corresponding sections.

After the description of the many successful developments, the last chapter covers an unfortunate and still largely unsolved problem with all gaseous detectors, the deterioration of performances, or ageing, with the long-term exposure to radiation.